An Electrochemical Sensing SoC for Autonomous Wound Monitoring

Maxx A. Seminario, Seth McRobert, Ayden Uerling, Paige Aberson, Sina Balkır
University of Nebraska-Lincoln,
Department of Electrical Engineering,
Lincoln, NE 68588-0511, USA
{mseminario2@huskers.unl.edu}

Joseph A. Schmitz
University of Nebraska-Lincoln,
School of Computing,
Lincoln, NE 68588-0150, USA
{jschmitz67@unl.edu}

Eric J. Markvicka
University of Nebraska-Lincoln,
Department of Mechanical and Materials Engineering,
Lincoln, NE 68588-0526, USA
{eric.markvicka@unl.edu}

***Abstract*— This paper presents the first integrated electrochemical sensing system-on-chip (SoC) for autonomous wound monitoring, integrating a custom potentiostat analog front end, 12-bit dual-slope ADC, RISC-V processor, and neural processing unit (NPU) on a single silicon die. Conventional wound monitoring approaches rely on multi-chip architectures that separate sensing from processing, resulting in high power consumption and connectivity dependencies that limit continuous wearable operation. This work achieves monolithic integration of the complete signal chain from electrochemical transduction to biomarker quantification by unifying analog sensing, digital processing, and machine learning. This integration enables wearable point-of-care wound monitoring by reducing power and connectivity requirements. Fabricated in 65 nm CMOS with a 1.5 mm × 1.0 mm die area, the SoC operates at 3.0 mW with 153 pA current resolution while performing cyclic voltammetry measurements to capture wound biomarkers including lactate, pH, and uric acid, with the integrated NPU converting electrochemical measurements into quantitative biomarker concentrations for continuous wound assessment.**

I. Introduction

Chronic wound management represents a significant healthcare challenge, affecting over 8.2 million patients annually with treatment costs exceeding $28 billion in the United States [1]. Effective wound healing depends on maintaining optimal biochemical conditions, including pH balance, bacterial load, and inflammatory biomarker levels [2]. Current wound assessment relies primarily on visual inspection and periodic sampling, which fails to capture the dynamic biochemical changes occurring during the healing process [3]. Continuous electrochemical monitoring offers a promising solution for real-time assessment of healing progression and early detection of complications [4].

Potentiostats enable electrochemical detection of wound biomarkers including lactate (tissue hypoxia), uric acid (inflammation), and pH (bacterial colonization) through voltammetric and amperometric methods [5], [6]. However, existing integrated potentiostat systems suffer from limitations: they rely on external processors for data analysis, lack intelligence to compensate for biological matrix effects, and utilize rigid form factors incompatible dynamic wound surfaces [7], [8]. While machine learning can address electrochemical sensing challenges, implementations require external computation, precluding autonomous operation [9], [10].

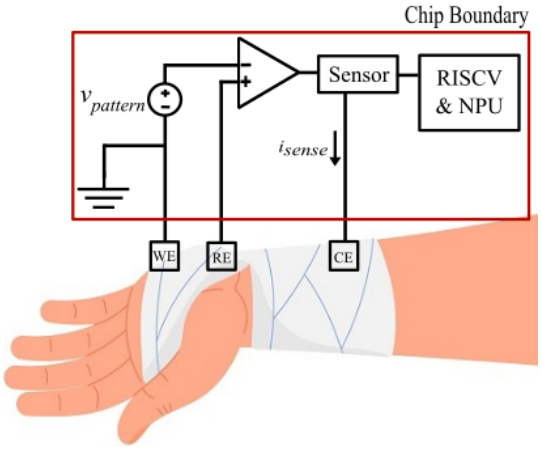

Fig. 1. Integrated electrochemical sensing SoC concept showing monolithic integration of potentiostat AFE, RISC-V processor, NPU for autonomous wound monitoring.

This work presents a novel system-level approach to electrochemical biosensing through the integration of analog sensing, embedded digital processing, and on-chip machine learning on a single silicon die. Unlike conventional multi-chip solutions, our SoC unifies the entire signal chain from electrochemical transduction to decision making, improving the size, weight, and power of wound monitoring solutions. Figure 1 illustrates the integrated concept, showing the electrochemical interface with three-electrode configuration, analog front end, and digital core. When considering the increased practicality of wireless powering and data transmission for this design, it provides a pathway for future bandages made with thinner and more flexible materials. The custom RISC-V processor, VestaRV [11], orchestrates measurements while the integrated NPU transforms raw electrochemical signatures into quantitative biomarker concentrations, enabling real-time wound assessment without any off chip processing.

II. System Architecture

The proposed electrochemical sensing SoC integrates three primary subsystems: a potentiostat analog front end (AFE) for electrochemical transduction, a custom RISC-V processor for system control, and a programmable NPU for intelligent

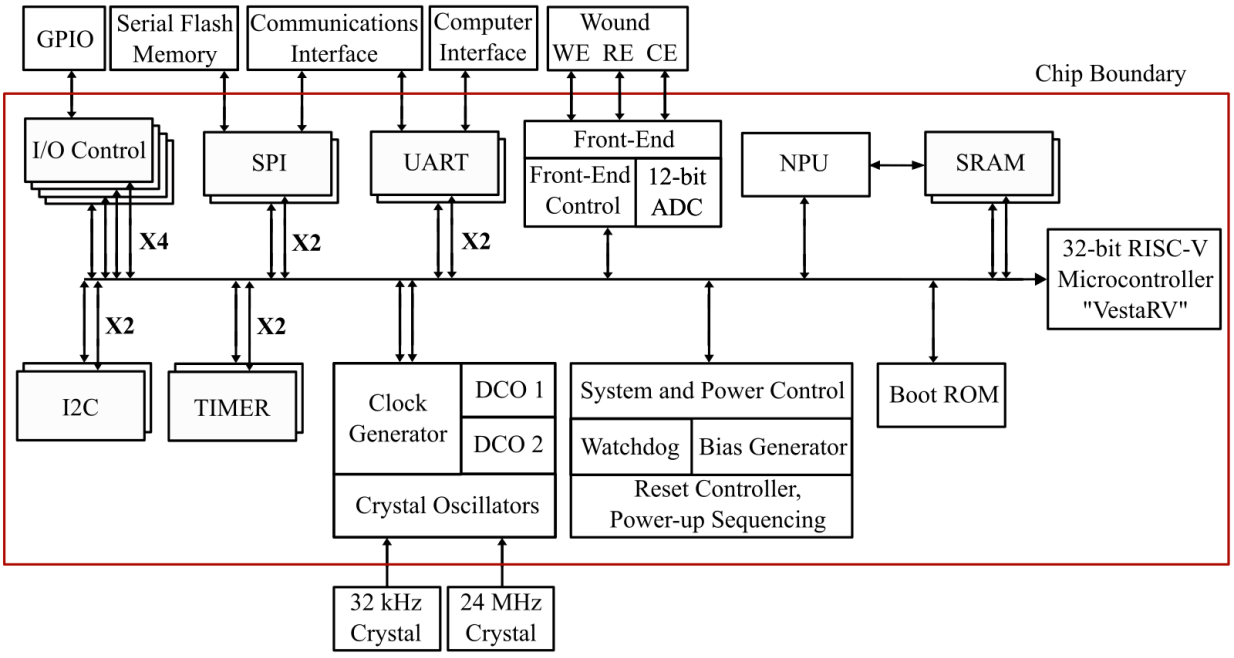

Fig. 2. System architecture of the integrated electrochemical sensing SoC showing the potentiostat front-end, VestaRV processor, and on-chip NPU.

signal processing. Figure 2 illustrates the complete system architecture with the key subsystems described below.

A. Potentiostat Analog Front-End

The potentiostat AFE implements a three-electrode electrochemical measurement system with programmable voltage control and current sensing capabilities. The design employs a p-type current mirror topology tailored for electrochemical measurements within the electrolysis window of water at approximately 1.5 V, beyond which water decomposition reactions preclude reliable electrochemical sensing.

The potentiostat AFE operates based on fundamental electrochemical principles governing the sensor-analyte interaction. For cyclic voltammetry measurements, the peak current i_p at the working electrode follows the Randles-Sevcik equation for diffusion-limited processes:

$$i_p = 0.4463(nF)^{\frac{3}{2}} AC \left(\frac{vD}{RT}\right)^{\frac{1}{2}} \tag{1}$$

where n represents the electron transfer number, F is Faraday's constant, A is the electrode area, C is the analyte concentration, v is the scan rate, D is the diffusion coefficient, R is the gas constant, and T is the absolute temperature. This relationship establishes the proportionality between peak current and the square root of scan rate, which the integrated digital processing section—comprising both the RISC-V processor and NPU —leverages for accurate concentration determination.

The potentiostat circuit topology, shown in Figure 3, operates through a feedback control system where operational amplifier A_1 maintains v_{re} at the programmed pattern voltage $v_{pattern}$ by generating output v_{fb} that drives the p-type current mirror gates. This feedback loop modulates cell current to

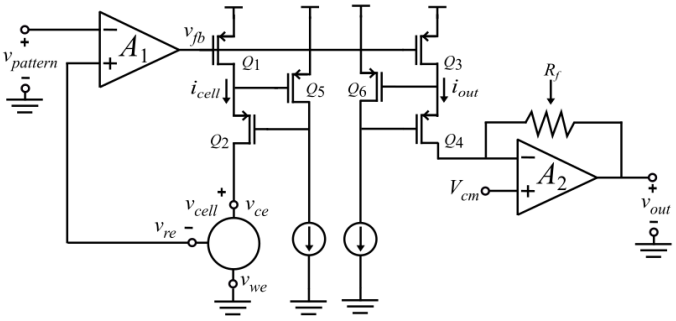

Fig. 3. Potentiostat circuit schematic featuring p-type current mirror, digitally programmable reference voltage $v_{pattern}$, and variable gain transimpedance amplifier with programmable feedback resistance R_f and common-mode bias voltage V_{cm}.

maintain $v_{re} = v_{pattern}$ while v_{ce} adjusts to accommodate the required current and v_{we} remains at signal ground. Transistors Q_5 and Q_6 regulate the drain voltages of mirror transistors Q_1 and Q_3, increasing output impedance and improving current mirror accuracy.

The transimpedance amplifier A_2 converts i_{out} to a voltage range suitable for the downstream 12-bit ADC. The non-inverting input of A_2 is biased at a DAC-generated common-mode voltage V_{cm} that establishes the operating point for both the TIA and downstream dual slope ADC. Programmable feedback resistor R_f is configurable from 0 Ω to 2 MΩ in 60 kΩ steps. This programmable gain accommodates cell currents from 153 pA to 20.8 μA while maintaining optimal ADC dynamic range utilization.

Combining the Randles-Sevcik equation with the transimpedance amplifier transfer function and solving for analyte concentration yields:

$$C = \frac{V_{cm} - V_{out,\,peak}}{0.4463(nF)^{\frac{3}{2}} A \left(\frac{vD}{RT}\right)^{\frac{1}{2}} R_f} \tag{2}$$

Where $V_{out,peak}$ is the output voltage corresponding to the peak current i_p measured during the voltammetric sweep. This equation enables the digital processing section to infer analyte concentration from the digitized output voltage measurements, with all electrochemical parameters and circuit gains accounted for. The programmable feedback resistance R_f allows dynamic range optimization based on expected concentration levels.

The AFE noise performance is designed to ensure the total integrated noise remains below half the quantization noise of the downstream 12-bit ADC. The primary noise sources in the potentiostat include the current mirror transistors Q_1 and Q_3, along with A_2. By increasing the size of Q_1 and Q_3 current mirror transistors, the input-referred current noise is reduced to 56.5 pA, maintaining noise below half the ADC quantization step.

B. Digital Processing Back-End

The on-chip NPU works in conjunction with the custom RISC-V processor to transform raw electrochemical measurements into actionable wound status assessments. VestaRV orchestrates the measurement sequence, extracting key features from *cyclic voltammograms* — electrochemical measurement where a triangular voltage waveform is applied to an electrode and the resulting current response is recorded — including peak currents, peak potentials, and time domain waveforms from the cell. These features may then be processed by the NPU to determine biomarker concentrations and wound healing status.

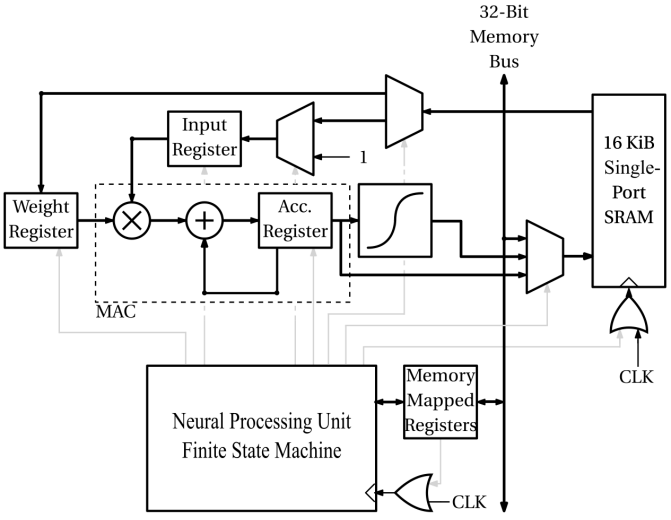

Fig. 4. Block diagram of the NPU showing single-port SRAM interface, MAC unit, and activation function module.

The NPU architecture in Figure 4 supports configurable network topologies in both number of hidden layers and neurons per layer, with programmable synapses enabling a wide range of network topologies. This configurability allows adaptation to different biomarker profiles and wound types. The implementation employs 32-bit fixed-point arithmetic (24-bit fractional, 8-bit signed integer) to maintain precision while minimizing power consumption and silicon area.

$$\phi(x) = \begin{cases} 0, & x \le -2^{\rho} \\ 2^{-1}(2^{-\rho}|x| - 1)^2, & -2^{\rho} < x < 0 \\ 1 - 2^{-1}(2^{-\rho}|x| - 1)^2, & 0 \le x < 2^{\rho} \\ 1, & x \ge 2^{\rho} \end{cases}$$

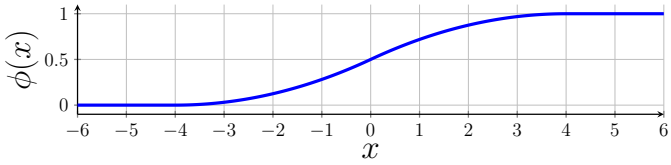

Fig. 5. Hardware-optimized piecewise quadratic activation function.

Figure 5 shows the hardware-optimized piecewise quadratic activation function [12], used by the neural network. This activation function requires only shift, multiply, and add operations, eliminating computationally expensive divisions while maintaining smooth gradients for stable training. The parameter ρ adjusts the dynamic range. The NPU supports both on-chip training for adaptive learning and off-chip training with weight loading for deployment of pre-trained models. To validate the NPU design, we evaluated its performance on the standard benchmark $f(x) = 2x^2 + 1$, showing mean squared error (MSE) convergence over 10,000 epochs with a 5-neuron hidden layer architecture, as shown in Figure 6.

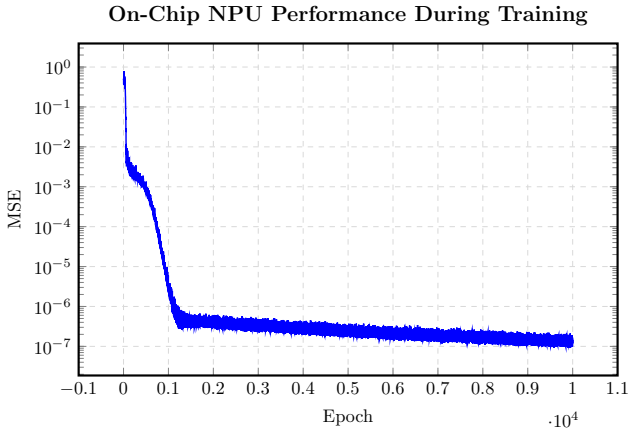

Fig. 6. NPU training on the standard $f(x) = 2x^2 + 1$ benchmark, showing MSE convergence.

III. Simulation Results

Figure 7 presents the simulation results of the proposed potentiostat circuit performing a cyclic voltammetry measurement. The top panel displays the applied triangular voltage waveform $v_{pattern}$, while the bottom panel shows control voltage v_{fb}, the electrochemical cell current i_{cell}, and the corresponding analog output voltage v_{out}. The circuit demonstrates excellent linearity with a normalized root mean square

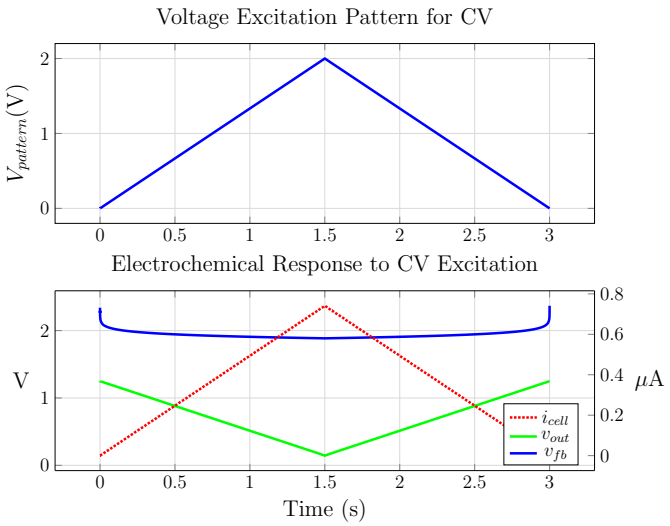

Fig. 7. Cyclic voltammetry measurement showing the applied voltage waveform and the corresponding electrochemical response.

TABLE I
PERFORMANCE SUMMARY AND COMPARISON

Parameter	**This Work**	**[7]**	**[8]**	**[13]**
Modality	CA/CV	CA/CV	CA/CV	CV/EIS
Sensitivity (pA)	56.5*	41	0.47	1.7
I_{max} (μA)	+20	$\pm$ 5	$\pm$ 20	-48/+16
Power (mW)	3.0†	16 m	9.3	1.0
Process (nm)	65	180	350	180
On-Chip DSP	VestaRV [11]	No	No	No
On-Chip ML	Yes	No	No	No

*AFE sensitivity; ADC quantization limits system to 153 pA
†AFE only: 258 μW

error of 0.025% between i_{cell} and v_{out}, meeting the performance requirements for accurate potentiostat measurements. Current clipping is observed when $v_{pattern}$ exceeds 2 V, attributed to the PMOS current mirror transitioning out of saturation. However, this limitation does not impact the intended application, as the circuit is specifically designed for electrochemical measurements within the water electrolysis window of approximately 1.5 V. Beyond this potential, water decomposition reactions dominate, making electrochemical sensing unreliable.

Table I demonstrates the capabilities of this architecture compared to state-of-the-art electrochemical sensing systems. This work uniquely integrates both a RISC-V processor and NPU on-chip, enabling autonomous biomarker quantification without the need for external processing.

The analog section, comprising the potentiostat AFE consumes 258 μW while achieving 56.5 pA input-referred current noise. The digital section contains the RISC-V processor, NPU, and all associated peripherals and memory blocks. The VestaRV core operates at 24 MHz with a power efficiency of 117 μW/MHz, consuming up to 2.8 mW during active operation, with total system power of 3.0 mW.

IV. PHYSICAL IMPLEMENTATION

The electrochemical sensing SoC was implemented with the complete physical layout shown in Figure 8. The design

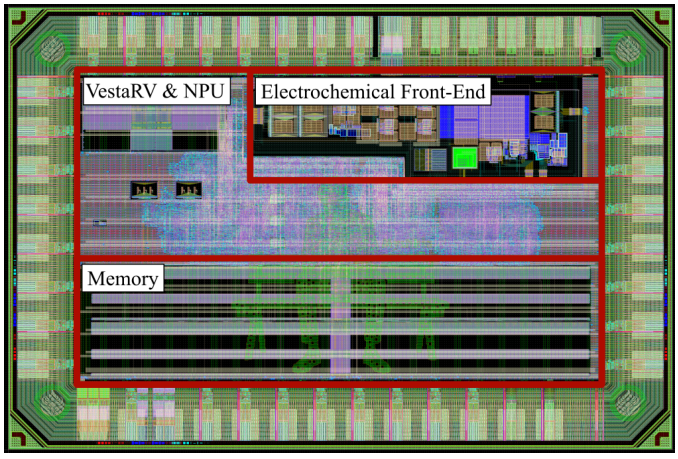

Fig. 8. Layout of the integrated electrochemical sensing SoC showing analog AFE, digital processor, and NPU, with dimensions of 1.50 mm × 1.00 mm in 65 nm CMOS.

is implemented in a 65 nm CMOS technology with overall dimensions of 1.50 mm $\times$ 1.00 mm. The VestaRV [11] core, microcontroller peripherals, and NPU are synthesized together as a unified digital block to optimize timing closure and minimize area overhead, occupying an area of 0.447 mm^2. The AFE occupies the occupies 0.135 mm^2 at the northeast of the chip.

V. CONCLUSION AND FUTURE WORK

Future work will involve encapsulation of the chip prototype for wearable integration using ultralow modulus silicone elastomer to ensure mechanical compatibility with dynamic wound surfaces. Based on our previous work [14]–[18], the SoC will be integrated into flexible bandage architectures using liquid-metal interconnects that maintain electrical connectivity during mechanical deformation. This approach will enable direct integration of the sensing system into conformable wound dressings for continuous monitoring applications.

The integration of analog sensing, embedded digital processing, and on-chip machine learning represents an advancement in autonomous wound monitoring. Unlike conventional approaches that rely on discrete components and external processing, this SoC achieves miniaturization by unifying the entire signal chain on a single 1.5 mm × 1.0 mm silicon die, small enough for direct integration into flexible bandages. The VestaRV processor orchestrates measurements and feature extraction, while the neural processing unit transforms electrochemical signatures into quantitative biomarker concentrations for lactate, pH, and uric acid. Critically, the monolithic integration reduces power consumption to 3.0 mW, enabling wireless power transfer for battery-free chemical sensing - a requirement for practical wearable deployment. By converging analog precision, digital control, and on-chip processing at the point of care, this system demonstrates progress toward wound management platforms where miniaturized diagnostic capabilities can be seamlessly integrated into bandages and powered wirelessly for continuous, unobtrusive patient monitoring.

REFERENCES

[1] C. K. Sen, "Human wounds and its burden: An updated compendium of estimates," *Advances in Wound Care*, vol. 8, no. 2, p. 39–48, Feb. 2019. [Online]. Available: http://dx.doi.org/10.1089/wound.2019.0946

[2] R. Derwin, "The role of ph and temperature as biomarkers of wound healing," Ph.D. dissertation, Royal College of Surgeons in Ireland, 2022.

[3] V. J Clemett, "Wound assessment and documentation: rationale and guidance," *British Journal of Nursing*, vol. 34, no. 15, p. S20–S26, Aug. 2025. [Online]. Available: http://dx.doi.org/10.12968/bjon.2024.0417

[4] M. I. Hossain, M. S. Zahid, M. A. Chowdhury, M. M. M. Hossain, N. Hossain, M. A. Islam, and M. H. Mobarak, "Smart bandage: A device for wound monitoring and targeted treatment," *Results in Chemistry*, vol. 7, p. 101292, Jan. 2024. [Online]. Available: http://dx.doi.org/10.1016/j.rechem.2023.101292

[5] J. Wang, "Electrochemical biosensors: Towards point-of-care cancer diagnostics," *Biosensors and Bioelectronics*, vol. 21, no. 10, p. 1887–1892, Apr. 2006. [Online]. Available: http://dx.doi.org/10.1016/j.bios.2005.10.027

[6] C. A. Sequeira, ""electrochemical wearable sensors for wound monitoring"," *Biomedical Journal of Scientific amp; Technical Research*, vol. 46, no. 4, Oct. 2022. [Online]. Available: http://dx.doi.org/10.26717/BJSTR.2022.46.007371

[7] Y.-C. Chen, S.-Y. Lu, and Y.-T. Liao, "A microwatt dual-mode electrochemical sensing current readout with current-reducer ramp waveform generation," *IEEE Transactions on Biomedical Circuits and Systems*, vol. 13, no. 6, p. 1163–1174, Dec. 2019. [Online]. Available: http://dx.doi.org/10.1109/TBCAS.2019.2936373

[8] S. S. Ghoreishizadeh, I. Taurino, G. De Micheli, S. Carrara, and P. Georgiou, "A differential electrochemical readout asic with heterogeneous integration of bio-nano sensors for amperometric sensing," *IEEE Transactions on Biomedical Circuits and Systems*, vol. 11, no. 5, p. 1148–1159, Oct. 2017. [Online]. Available: http://dx.doi.org/10.1109/TBCAS.2017.2733624

[9] G. F. Giordano, L. F. Ferreira, R. S. Bezerra, J. A. Barbosa, J. N. Y. Costa, G. J. C. Pimentel, and R. S. Lima, "Machine learning toward high-performance electrochemical sensors," *Analytical and Bioanalytical Chemistry*, vol. 415, no. 18, p. 3683–3692, Jan. 2023. [Online]. Available: http://dx.doi.org/10.1007/s00216-023-04514-z

[10] P. Puthongkham, S. Wirojsaengthong, and A. Suea-Ngam, "Machine learning and chemometrics for electrochemical sensors: moving forward to the future of analytical chemistry," *The Analyst*, vol. 146, no. 21, p. 6351–6364, 2021. [Online]. Available: http://dx.doi.org/10.1039/D1AN01148K

[11] M. A. Seminario, "Vestarv: A risc-v processor core," https://github.com/maxxseminario/VestaRV, 2026.

[12] E. López-Rubio, F. Ortega-Zamorano, E. Domínguez, and J. Muñoz-Pérez, "Piecewise polynomial activation functions for feedforward neural networks," *Neural Processing Letters*, vol. 50, no. 1, p. 121–147, Jan. 2019. [Online]. Available: http://dx.doi.org/10.1007/s11063-018-09974-4

[13] Y.-J. Lin, W.-C. Liu, Y.-C. Huang, Y.-J. Huang, Y.-H. Yeh, M.-H. Chang, S.-P. Lin, Y.-C. Liao, and Y.-T. Liao, "A multimodality electrochemical and impedance spectroscopy system-on-a-chip with temperature sensing and impedance-boosting techniques," *IEEE Transactions on Biomedical Circuits and Systems*, vol. 17, no. 4, p. 857–871, Aug. 2023. [Online]. Available: http://dx.doi.org/10.1109/TBCAS.2023.3287835

[14] M. Palvanova, P. McManigal, G. Fredrickson, and E. J. Markvicka, "Laser micromachining of liquid metal patterns for stretchable electronic circuits," *Advanced Materials Technologies*, 2025.

[15] E. Markvicka, G. Wang, Y.-C. Lee, G. Laput, C. Majidi, and L. Yao, "Electrodermis: Fully untethered, stretchable, and highly-customizable electronic bandages," in *Proceedings of the 2019 CHI Conference on Human Factors in Computing Systems*, ser. CHI '19. ACM, May 2019, p. 1–10. [Online]. Available: http://dx.doi.org/10.1145/3290605.3300862

[16] C. Pan, K. Kumar, J. Li, E. J. Markvicka, P. R. Herman, and C. Majidi, "Visually imperceptible liquid-metal circuits for transparent, stretchable electronics with direct laser writing," *Advanced Materials*, vol. 30, no. 12, Feb. 2018. [Online]. Available: http://dx.doi.org/10.1002/adma.201706937

[17] M. D. Bartlett, E. J. Markvicka, and C. Majidi, "Rapid fabrication of soft, multilayered electronics for wearable biomonitoring," *Advanced Functional Materials*, vol. 26, no. 46, p. 8496–8504, Sep. 2016. [Online]. Available: http://dx.doi.org/10.1002/adfm.201602733

[18] M. A. Seminario, A. Uerling, S. Balkır, M. W. Hoffman, J. A. Schmitz, and E. J. Markvicka, "A fully flexible temperature sensor for wearable applications," in *2025 IEEE International Symposium on Circuits and Systems (ISCAS)*, pp. 1–5. [Online]. Available: https://ieeexplore.ieee.org/document/11043365